9th International Conference on Numerical Ship Hydrodynamics
Ann Arbor, Michigan, August 5-8 2007

Numerical Simulation of Flow over Fully Appended ONR Body-1 with Overset Grid Scheme

Lawrence P. Mulvihill, Cheng-I Yang
(Naval Surface Warfare Center Carderock Division)

ABSTRACT

In order to simplify the construction of the computational grid about complex geometries and to enable the numerical simulation of relative motion between components, an overset grid assembler SUGGAR has been integrated with an existing RANS flow solver UNCLE. This modified flow solver with overset capability allows different flow regions to have their own separate grid that is adaptive to the particular feature of that region. The complete flow field is then made up of a group of overlapping sub-grids. A grid assembler is then used to provide the flow solver with the connectivity information among the sub-grids and the interpolation stencils of the boundary nodal points. To demonstrate the flexibility, feasibility and accuracy of the overset grid scheme, numerical simulations of flow over ONR-Body-1 were performed.

ONR-Body-1 is a fully appended submarine model. It was built with the intention to study the complicated flow field about a submarine during maneuvering. It was tested in the tow tank at NSWCCD. Three-dimensional velocity components around the body were measured with the SPIV technique, the force and moment coefficients were obtained through block gages.

Comparisons of simulation and experiment and discussion are presented in the report.

NOMENCLATURE

A_{ref}	Reference area, $(L_{ref})^2$
C_P	pressure coefficient $\frac{P}{\frac{1}{2}\rho V_{ref}^2}$
d	distance from the wall
F	Force on body, in x,y or z direction
K', M', N'	Moment coefficients $\frac{M}{\frac{1}{2}\rho V_{ref}^2 L_{ref} A_{ref}}$, roll, pitch and yaw.
M	Moment about the center of gravity, roll, pitch or yaw
L_{ref}	Reference length, hull length
P	Static pressure
Re	Reynolds number $(V_{ref} L_{ref})/\upsilon$
V_{ref}	Reference velocity , ship speed
x,y,z	Cartesian coordinate system, origin located at the forward perpendicular along the center line of the hull
X', Y', Z'	Force coefficients $\frac{F}{\frac{1}{2}\rho V_{ref}^2 A_{ref}}$, in x,y, z directions
y^+	Turbulence coordinate, $d\sqrt{\tau_w/\rho}/\upsilon$
τ_w	shear stress at wall
ρ	Density
υ	kinematic viscosity

INTRODUCTION

Finite difference and finite volume methods are well developed for the approximate solutions of a system of partial differential equations, such as Reynolds-averaged Navier-Stokes equations. Commonly, the solution domain is first discretized with inter-connected grid points that are well ordered. The structured nature of the grid points makes it easier to implement the high-order approximation of the differential equations. In the case of solving viscous flow problem, near the solid surface, the grid can be easily clustered so that the boundary layer profile can be sufficiently resolved. However, for a more complex geometry, where a complicated flow pattern is anticipated, a highly skewed grid is difficult to avoid. In general, the solutions supported by skewed grids are less accurate. Generating an unstructured grid system for complex geometries is relatively easier but not necessarily trivial. Besides, because of the unstructured grid system is not well ordered, higher-order approximation is not easy to enforce [Steger, Benek, 1987]. An alternative for dealing with the complex geometries is the use of a composite grid system, in which individual structured grids representing different regions are overset on each other. Such a grid system also becomes very desirable when treating the components that are moving with respect to each other. The connectivity information among the grids and the interpolation stencils for the interface boundary nodes can be identified and determined for the use of the flow solver. Clearly, the overset grid approach requires additional effort for grid assembling, but in return, the process of construction of the grid becomes simplified, especially when complex geometries are involved. In addition, there is more control of grid quality.

Motivated by those potential benefits, Steger, Dougherty and Benck [Steger, Dougherty, Benck, 1983] first introduced the overset grid concept in 1983. Since then, much research efforts, especially those provided by the Integrated Wing Design (IWD) element of the NASA's Advanced Subsonic Technology (AST) program, were directed to the development of the overset CFD software. More recently, a successful compressible flow simulation of a Boeing 777 aircraft in landing configuration was reported [Rogers, Roth., Cao, Slotnick, Whitlock, Nash, Baker, 2000]. For this particular computation, 22.4 million grid points within 79 overset zones were used. To support and facilitate the computations of such high degree of complicity, several grid-assembling utilities have been developed: (1) OVERGRID, to generate and manipulate the overset grids [Chan, Gomez, Rogers, Buning, 2002.], [Chan,2002]. (2) PEGASUS, to perform hole-cutting and to provide the connectivity information among overlapping grids [Suhs, Rogers, Dietz, 2002], (3) FOMOCO, to integrate force and moment on the solid surfaces that are covered with overlapping grids [Chan, Buning, 1996]. Those utility programs have become workhorses for many CFD applications in NASA, universities and industries.

In the field of incompressible flow, Kim simulated rotor blade tip vortex cavitation with a overset grid approach [Kim, 2002]. A dense and high quality grid is placed around the blade tip region to resolve the fine flow structure of the tip vortex. Wilson et al used the same method to simulate the large amplitude motion and maneuvering for surface ship [Wilson, Carrica, Hyman, Stern, 2004], There, the ability to use the local refinement for the Kelvin wave system with the overset grid is illustrated. The details of the method are described in a reference by Peterson et al [Paterson, Wilson, Stern, 2004]. In essence, this incompressible RANS solver CFDSHIP-IOWA is based on pressure implicit with split operator (PISO) algorithm. The grid assembling was accomplished with the utility programs developed at NASA as described earlier.

It is reasonable to conclude that the Chimera grid embedding technique is desirable and mature for CFD applications. The fact that the grid assembling process can be modularized, makes adding the overset capability to a flow solver extremely feasible. It is a logical and natural way to bring the existing and validated flow solver to a new and higher level of application. R. Noack has developed an interface routine DiRTlib that makes the process of adding the overset capability to a flow solver extremely transparent [Roack, 2005]. The DiRTlib is installed in the flow solver UNCLE, this new version with overset capability is termed as UNCLE-overset. A similar endeavor has been carried out at PSU, and some numerical results were reported [Boger, Dryer, 2006]. This report describes and discusses the flow solver, the grid assembler and the numerical simulations performed for the validation purpose. New software USURP designed by Boger to integrate the forces and moments on overset grids is presented in the report.

The FLOW SOLVER – UNCLE-overset

UNCLE was developed at Mississippi State University for solving the three-dimensional incompressible Reynolds-average Navier-Stokes equations [Taylor, 1991]. Artificial compressibility is used to couple the pressure and velocities [Chroin, 1967], with upwind wind flux-difference splitting approximation for the convective terms [Roe, 1981]

and second order central differencing approximation for the diffusive terms. With this approach, the RANS equations are treated like a system of hyperbolic equations. UNCLE has accumulated certain amount validation throughout the years. To enhance its accuracy, a fifth-order stencil was added to approximate the convective terms [Yang, Jiang, Chesnakas, Jessup, 2004]. To perform the overset grid calculation, some modifications about the matrix of the system of equations of the solver are needed for the fringe and the hole points: (1) set the off-diagonal elements to zero, (2) set the diagonal elements to unity, and (3) set the residuals to zero. As a result, the solutions on those points are not updated during iterations. Interface subroutines are also implemented to UNCLE to facilitate the overset calculation.

For turbulence modeling, there are two options in the code: the k-ε and q-ω models. The results presented here are based on the latter model.

THE GRID ASSEMBLER – SUGGAR

The overset grid utilizes a set of overlapping grids to discretize the domain and uses interpolation at appropriate points to couple the solution on the different grids. Any points that lie outside the domain of interest, for example, the grids discretizing the submarine hull that lie interior of the sail or the appendages, are marked for exclusion for the computation and are termed "hole point". Points that surround the hole points become new inter-grid boundary points, which are called fringe or receptor points, and require boundary values to be applied. The boundary values required by a receptor point are provided by interpolating from a donor grid that overlaps the region. The definition of which points are hole points, receptor points along with their corresponding donor members is termed domain connectivity information and is provided by an overset assembly code, SUGGAR (Structured, Unstructured, Generalize overset Grid AssembleR). SUGGAR is designed by R. Noack [Noack, 2005], to produce overset composite grid assemblies of structured, unstructured, and/or generalized grids for node centered or cell centered flow solvers.

THE INTERFACE LIBRARY – DIRTLIB

The domain connectivity information obtained from SUGGAR is transformed to the solver, and the hole points, the receptor points are properly identified. The solution on appropriate locations in the donor grids is extracted and multiplied by the interpolation coefficient to produce the value required for the receptor locations. The interpolated values are applied at the receptor locations as Direchlet boundary values. The interpolation and distribution processes are performed by the DiRTlib (the Donor interpolation Receptor Transaction library). DiRTlib is developed by R. Noack[Noack, 2005]. The library simplifies the addition of an overset capability by reducing the amount of code the flow solver developer must write.

THE EXPERIMENT – FLOW ABOUT ONR-BODY-1

The submarine model used in the experiment is DTMB #5484 with a length of 5.27 m, a diameter of 0.47m. The center of gravity is located at 2.35m (five times the body diameter) aft of the forward perpendicular along the centerline of the hull. The sail has a NACA 0014 section with a chord length of 0.57 m and an aspect ratio of 0.27. The leading edge of the sail is located at x/L =0.2. The appendages, two rudders and two stern planes, are identical in shape and size. They have NACA 0018 sections, with a chord length of 0.18 m and aspect ratio of 1.2. It is configured as ONR-Body-1 [Fu, Atsavapranee, Hess, 2002]. The tow speed is 5 knots. The corresponding Reynolds number, based on the body length, is 13.5 million. The details of the test procedure and setup can be found in reference [Atsavapranee, Forline, Fry., Hamiliton, Percival, Sung, 2004]

By using stereo particle image velocimetry (SPIV) flow patterns with all three velocity-components around the model were gathered and analyzed for three model configurations: bare hull, bare hull with sail, and fully appended. The main purpose of the tests is to correlate to the measurements of flow-field, pressure distribution and overall forces and moments on the model to explain the effects of the dominant flow features such as the sail tip vortex on the flow development and the cross flow separation around the hull. Test data are well documented and are suitable for the validation of the newly modified and assembled UNCLE-overset code. At present, only a portion of the test matrix will be numerically simulated.

GRID CONSTRUCTION

The ONR-Body-1 contains all the essential components of an operational submarine except the propulsor, namely, the hull, the rudders and the stern planes. The construction of the overlapping grids for the computational domain is greatly simplified since there is no requirement to match the interface grid points, only sufficient overlapping between grids is necessary.

Based on the same geometrical database, each grid about each individual component can be generated independently. The Hull surface is first discretized with a network of four sided surface panels. The nodes of the panels lie on the surface definition. The panel density can be varied to suit the local surface curvature or the intersections with the other components. The body-conforming volume grids are then created from the surface grids by hyperbolic marching [Chan, 1993]. The marching process can be control by specifying the off body distance of the first grid point and the expansion ratio. The hull grid is subdivided into a set of overlapping grids, for parallel processing. A simpler and courser far field grid in the spherical form that is overlapping with the hull grid is generated to extend the far field boundary to three body lengths upstream and downstream. The sail grid itself is made of a set of overlapping grids. It has: (1) a collar grid that covers the sail/hull intersection region, (2) a wing grid that covers most of the sail region and (3) a tip grid that wraps around the tip of the sail. Such grid topology was suggested for wing/fuselage configurations in reference [Roger, Roth, Cao, Slotnick, Whitlock, Nash, Baker, 2000]. Once the sail grid is completed, it can be added to the hull grid to form the sail/hull configuration. This procedure can be repeated by adding the grids for rudders and stern planes to the hull grid to form computational grids for a fully appended configuration.

Upon the application of the grid assembling code SUGGAR, the hull grid points that lie within and immediately surrounding the sail/appendages are removed, and the fringe points, donor points and the hole points are identified. Furthermore, the interpolation stencils associated with each fringe point are computed and stored as part of the connectivity information.

Figure 1 shows the fully appended ONR Body-1. Notice that there are no fillets in the juncture regions.

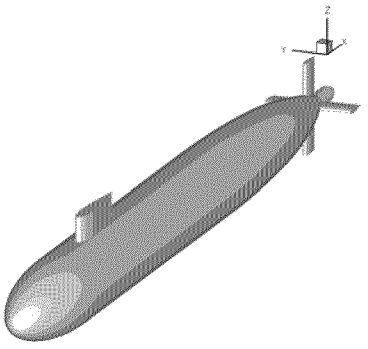

Figure 1: Fully appended ONR Body-1.

Figure 2 shows the overlapping surface grids at the sail/hull juncture region. It can be seen that the sail grid is composed of a collar grid, a wing grid and a tip grid. Similarly, Figure 3 shows the overlapping surface grids at the appendages/hull juncture region. Clearly all the surface grids are near orthogonal and well define, and at the overlapping regions, the grids of different components are about the same size.

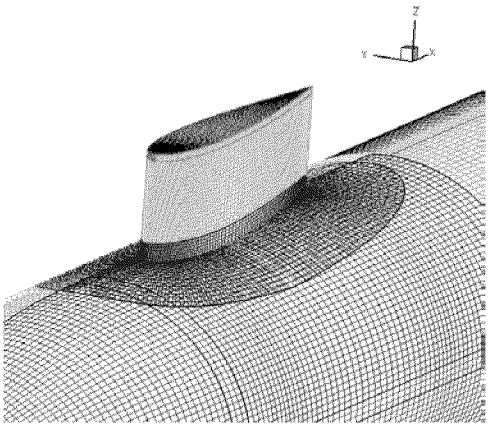

Figure 2: Overlapping surface grids at sail/hull juncture region.

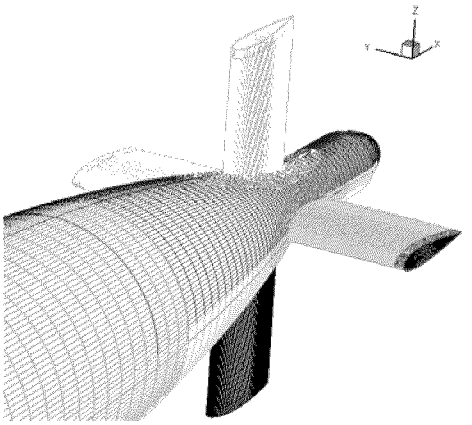

Figure 3: Overlapping surface grids at appendages/hull juncture region.

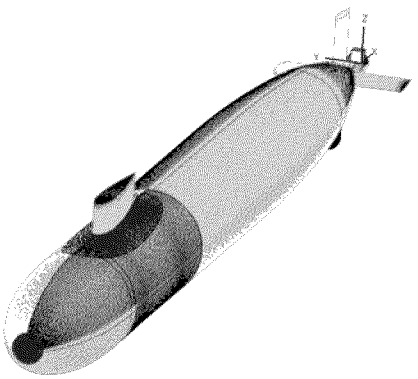

Figure 4: Complete overlapping surface grids on ONR Body-1.

Figure 4 shows the complete surface grids for the fully appended configuration. The grid density is higher near bow and stern of the hull so that the surface curvature is well represented. For the same reason, the grids are clustered near the leading and trailing edges of the sail and appendages.

Figure 5 shows the contour of the local surface panel area of the sail/hull configuration, the length scale is normalized by the hull length. The contour reflects the distribution of the surface grid density; surface panel area is smaller at the region where the radius of curvature is small.

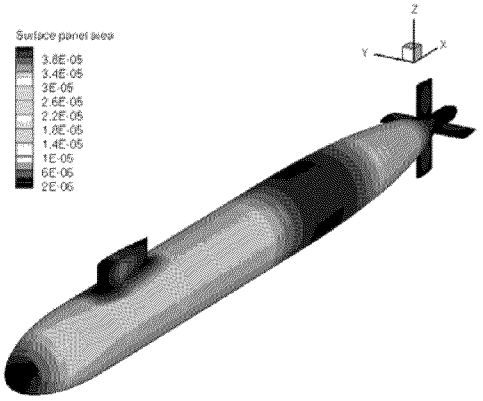

Figure 5: Contour of local surface panel area.

Figure 6 shows that the sail and appendage grids embed in the hull grid. Figure 7 shows that the hull grid embeds in the far field grid.

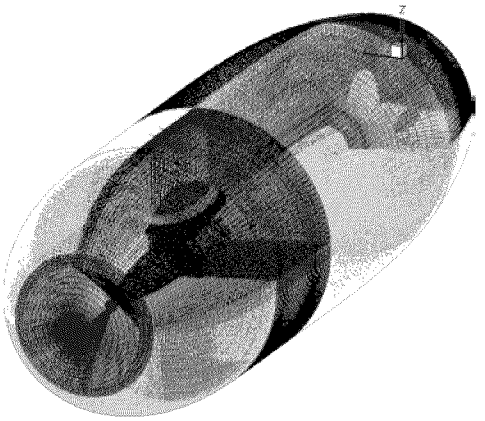

Figure 6: Sail and appendages grids imbedding in the hull grid.

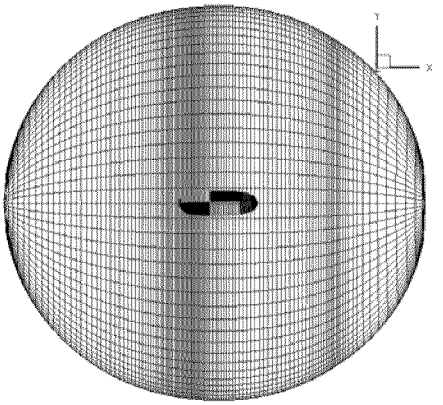

Figure 7: Hull grid embedding in far field grid.

The total number of grid points is about 10 millions for a fully appended configuration. For the purpose of multi-processing, the grid systems are divided into blocks; each block has approximately quarter million nodes. Twenty-two and thirty-four blocks are used for the sail/hull and the fully appended case, respectively.

NUMERICAL SCHEME

The numerical solver used in present simulations is based on the CFD code UNCLE developed at MSU. It is based on a three-dimensional incompressible Navier-Stokes equation expressed in the conservative law form. The equations are coupled with the continuity equation through the artificial compressibility. The diffusive terms are discretized with a central differencing scheme, and the

convective terms are discretized with the Roe's flux-difference splitting scheme [Roe, 1981]. For the steady state simulation, a first order Euler backward approximation is used to represent the time derivative. To accommodate the rotational motion, the equations of motion are first formulated in a rotating coordinate system attached to the moving body, but are then recast in the absolute-flow variables. Such a formulation is popular in turbomachinery applications. It is believed that such formulation allows more accurate calculation of flux in the finite volume method.

The Navier-Stokes equations of the three-dimensional, time dependent, incompressible flow can be written in a curvilinear coordinate and in a strongly conservative law form as

$$\left(\frac{Q}{J}\right)_t + (E - E_v)_\varepsilon + (F - F_v)_\eta + (G - G_v)_\varsigma = 0 \quad \textbf{(1)}$$

Where $Q = (\rho, u, v, w)^T$

$$\text{and} \quad \begin{bmatrix} E \\ F \\ G \end{bmatrix} = \begin{bmatrix} \frac{\varepsilon_x}{J} & \frac{\varepsilon_y}{J} & \frac{\varepsilon_z}{J} \\ \frac{\eta_x}{J} & \frac{\eta_y}{J} & \frac{\eta_z}{J} \\ \frac{\zeta_x}{J} & \frac{\zeta_y}{J} & \frac{\zeta_z}{J} \end{bmatrix} \begin{bmatrix} E^* \\ F^* \\ G^* \end{bmatrix} \qquad (2)$$

with the inviscid fluxes

$$\begin{aligned} E^* &= \left(\beta u, u^2 + p, uv, uw\right)^T \\ F^* &= \left(\beta v, uv, v^2 + p, vw\right)^T \\ G^* &= \left(\beta w, uw, vw, w^2 + p\right)^T \end{aligned} \qquad \textbf{(3)}$$

and shear fluxes

$$E_v, F_v, G_v$$

β is the artificial compressibility which connects the continuity equation with the momentum equation, J is the transformation Jacobian which relates the physical domain to the computational domain, and $\varepsilon_x, \varepsilon_y, \varepsilon_z, \eta_x, \eta_y, \eta_z, \zeta_x, \zeta_y, \zeta_z$ are transformation metrics.

In order to apply Roe's concept of flux differencing to the convective and pressure differentiation terms, the Reynolds number is assumed high and approaching infinite. The shear fluxes (E_v, F_v, G_v) are then relatively small in comparison with their corresponding inviscid fluxes (E, F, G). It can then be assumed that the waves that travel across a cell face are normal to the face. Subsequently the three-dimensional system of partial differential equations is spatially split into three quasi one-dimensional conservative laws

$$\left(\frac{Q}{J}\right)_t + H_\theta = 0, \qquad \textbf{(4)}$$

where θ is ε, η, or ζ, and H is E, F or G. Defining computational cells with their centroids at m (m=i, j, or k), and their cell interfaces at m±1/2, an implicit discrete approximation to Equation 4 can be written as

$$\left[\left(\frac{I}{\tau J}\right) + D_m \Delta_m\right] \Delta Q^n + \Delta_m H^n = 0, \qquad (5)$$

where τ is time step size, $\Delta Q^n = Q^{n+1} - Q^n$ and $\Delta_m H = \left[H_{m+1/2} - H_{m-1/2}\right]/\Delta\theta$ and $D = \partial H/\partial Q$ the flux Jacobian. For the construction of an approximate Riemann solver for the initial value problem in Equation 5, the flux at the cell interface m+1/2 that separates the right from the left traveling wave, can be define as

$$H^n_{m+1/2} = H^n_m + (\Delta H^-_{m+1/2})^n, \qquad (6)$$

or

$$H^n_{m+1/2} = H^n_{m+1} - (\Delta H^+_{m+1/2})^n, \qquad \textbf{(7)}$$

or the simple average of Equations 6 and 7. At present calculation, Equation 6 is used, since it has less operation count. In Equations 6 and 7, the superscript – and + of the flux differencing term represents the right and the left traveling wave across the interface m+½, respectively. That is

$$\left(\Delta H^-_{m+1/2}\right)^n = \left[R\Lambda^- R^{-1}(Q^R_{m+1} - Q^L_m)\right]^n, \qquad (8)$$

and

$$\left(\Delta H^{+}_{m+1/2}\right)^{n} = \left[R\Lambda^{+}R^{-1}\left(Q^{R}_{m+1} - Q^{L}_{m}\right)\right]^{n}, \qquad (9)$$

with R, R^{-1} represent right and left eignvector of the eigen system of flux Jacobian D, respectively, Λ^{+}, Λ^{-} represent positive and negative eigen value of the system, respectively, and Q^{R}_{m+1}, Q^{L}_{m} represent the dependent variable to the right and the left of the interface, respectively. For the first order approximation, $Q^{R}_{m+1} = Q_{m+1}$ and $Q^{L}_{m} = Q_{m}$.

To evaluate Equation 6 numerically, a Roe's [Roe, 1981] mean value matrix $D_{m+1/2} = D(Q_m, Q_{m+1})$ is introduced with the following properties;

$$D_{m+1/2}\Delta_{m+1/2}Q = \Delta H_{m+1/2}, \qquad (10)$$

and

$$D(Q_m, Q_{m+1}) = D_m, \quad \text{if } Q_m \to Q_{m+1}. \qquad (11)$$

The conditions in Equations 10 and 11 are to ensure that the solution to Equation 5 is conservative in space. For the incompressible flow, the only state of the dependent variable Q that satisfies these properties is the simple average of the Q^{R}_{m+1}, and Q^{L}_{m}. Accordingly, the first term on the right hand side of Equation 6, H^{n}_{m}, is computed with the metrics evaluated at the interface m+½ and the dependent variable Q evaluated at centroid m, that is Q=Q^{L}_{m}. For the second term on the right hand side of Equation 6, $(\Delta H^{-}_{m+1/2})^{n}$, the eignvectors and the eignvalues R, R^{-1}, Λ^{-}, are evaluated with the metrics and the dependent variable defined at the interface m+½, that is Q=$\frac{1}{2}\left(Q^{R}_{m+1} + Q^{L}_{m}\right)$.

To enhance the accuracy of the solution, Van Leer's [van Leer, 1974] MUSCL (monotone upstream-centered scheme for conservation laws) approach is adopted. The dependent variables to the right and to the left of the interface of the cell are reconstructed as

$$Q^{R}_{m+1/2} = Q_{m+1} - \frac{\varphi}{4}\begin{bmatrix}(1-\kappa)(Q_{m+2} - Q_{m+1}) \\ -(1+\kappa)(Q_{m+1} - Q_{m})\end{bmatrix} \qquad (12)$$

and

$$Q^{L}_{m+1/2} = Q_{m} + \frac{\varphi}{4}\begin{bmatrix}(1-\kappa)(Q_{m} - Q_{m-1}) \\ +(1+\kappa)(Q_{m+1} - Q_{m})\end{bmatrix}. \qquad (13)$$

If φ=0, the Equations 12 and 13 recover the first order approximation. If φ=1 and κ= -1, the approximation is second order. If φ=1 and κ=1/3, the approximation is third order. An alternative approach to the reconstruction is to apply the stencil shown in Equations 12 and 13 to the characteristic variables W in the computational space, where $W = R^{-1}Q$. Once $W^{R}_{m+1/2}$ and $W^{L}_{m+1/2}$ are obtained, the independent variables $Q^{R}_{m+1/2}$ and $Q^{L}_{m+1/2}$ can be recovered by pre-multipling $W^{R}_{m+1/2}$ and $W^{L}_{m+1/2}$ with the right eignvector R computed at the interface m+1/2. This reconstruction process, identified here as weighted MUSCL here, requires higher operation count, but it takes the coordinate non-uniformity, stretching and orientation into account, since the characteristic variables are function of grid position and matrix. The scheme described here, has been used to compute the flow in linear cascade with tip clearance [Yang, 2002]. Similarly, a fifth order stencil, suggested by Rai [Rai, 1987] and used by Rogers and Kwak [Rogers, Kwak, 1990], is derived and applied to the characteristic variables here. That is

$$W^{R}_{m+1/2} = W_{m+1} + \frac{1}{60}[+2\Delta_{m+5/2}W - 11\Delta_{m+3/2}W - 24\Delta_{m+1/2}W + 3\Delta_{m-1/2}W] \qquad (14)$$

and

$$W^{L}_{m+1/2} = W_{m} + \frac{1}{60}[-2\Delta_{m-3/2}W + 11\Delta_{m-1/2}W + 24\Delta_{m+1/2}W - 3\Delta_{m+3/2}W] \qquad (15)$$

The weighted MUSCL schemes described here are implemented in the UNCLE code for present calculations.

The numerical viscous fluxes defined in Equation (1 can be obtained through central differencing technique without using the thin-layer approximation. The differencing equations that represent the full Navier-Stokes equation formulated in conservation form can then be assembled. The system of equations is solved with Newton iteration method. q-ω type turbulence

NUMERICAL RESULTS

Since the grid systems on solid surface are overlapping, direct integrating forces over the surface would result in the overlapping regions being counted more than once, special attentions are needed. At present, the force integration routine FOMOCO [Chan, Buning, 1996] was used. The FOMOCO utility is a stand alone software package for computing flow coefficients (force, moment, and mass flow rate) on a collection of overset surfaces with accurate accounting of the overlapped zones. The computational results presented here are for the cases of flow over the hull/sail combination and fully appended configuration at various yaw angles. To facilitate the study and the discussion of the forces acting on the body, the body is divided into several zones, those are, the bow, the mid-body, the stern, the sail and the appendages as shown in Figure 8. The bow section extends from the forward perpendicular to x=0.129L, from there, the mid-body extends to x=0.618L. The section beyond x=0.618L is defined as stern section.

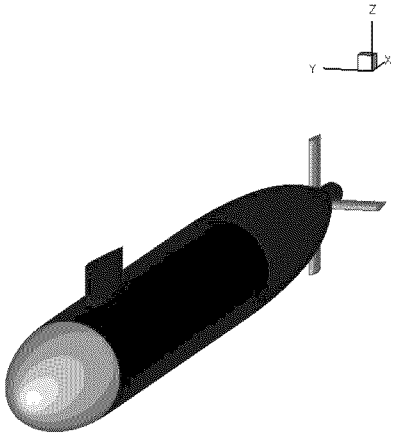

Figure 8: Domain division for force and moment integration.

At the zero degree angle of attack, the axial velocity contour along the hull for the sail/hull and the fully appended configurations are shown in Figure 9. The axial locations, where the axial velocity contours are shown, are x = 0.4L, 0.5L, 0.6L, 0.7L, 0.8L, 0.9L and 0.99L, respectively. Figure 9 shows that, at the straight-ahead condition, the axial velocity profile upstream of x=0.9L is not affected by the present of appendages. The shape of the contours suggests the existence of a horseshoe vortex behind the sail. The turbulence coordinate y+ of the first off body grid point over the body surface, for the fully appended case at Reynolds number at 13.5 million, is shown in Figure 10. Over the majority of the surface, the value of y+ is under 0.005. This is an indication that there is a sufficient number of grid points near the body surface for the q-ω turbulence model to resolve the sub layer. Forces integration over the bow sections for the sail/hull and fully appended configurations produces identical results. The same conclusion is observed for the mid-body sections and the sail sections. In comparison, the stern section for the fully appended configuration produces slightly more drag, because it has less pressure recovery.

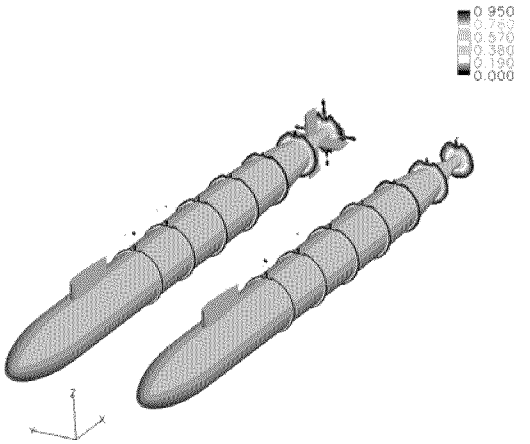

Figure 9: Axial velocity contour along the hulls at 0° angle of attack.

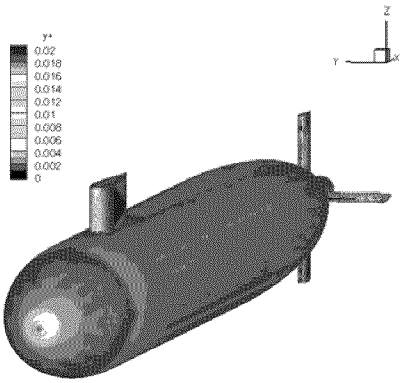

Figure 10: The turbulence coordinate y+ for the fully appended configuration at 0° angle of attack.

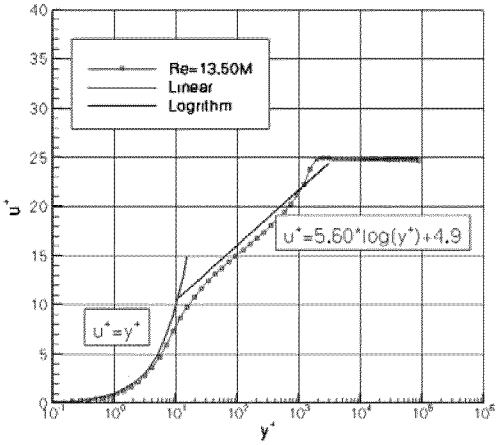

Figure 11: Law of wall plot at hull, X/L=0.365

The axial velocity profile, in term of the turbulence coordinates y^+ and u^+, at the mid-body section of the hull where X/L = 0.365, is shown in Figure 11. At Reynolds number 13.5 million, there are about 10 grid points within y^+=1.0. The present grid system is suitable for computations at a much higher Reynolds number. The constant 4.9 associated with the logarithmic function in Figure 11 is for the smooth surface.

The computed total drag coefficient for the sail/hull configuration is 0.000800. The contributions from the bow, the mid-body, the stern and the sail are 14.375%, 51.00%, 29.50%, and 5.125% of the total, respectively. The pressure drag contributes 9.875% of the total and the viscous drag contributes 90.125% of the total. The computed total drag for the fully appended configuration is 0.000915. The contributions from the bow, the mid-body, the stern, the sail and the appendages are 12,677%, 45.136%, 28.087%, 4.481% and 9.727%, respectively. The pressure drag contributes 13.989% and the viscous drag contributes 86.011% of the total.

Figure 12 shows the axial velocity contour along the fully appended hull at 12° yaw. The axial locations for the contours are x/L=0.3, 0.4, 0.5, 0.6, 0.7, 0.8 and 1.0. The contours indicate the passage of the vortex shedded from the sail tip, the primary and the secondary separation vortices from the hull surface. Figure 13 shows where the streamlines emit from the separation lines on sail and hull surfaces. The sail tip vortex induces a hull bound circulation that has equal strength but opposite in direction. When this circulation interacts with the cross flow caused by the yaw, a downward force acting on the stern is generated. This induced force causes the bow to pitch upward. When the yaw angle increases, the flow on the leeward side starts to separate. There are two primary separation lines, one upper and one lower as shown in Figure 13. Due to the interaction with the hull bound circulation, the strength of upper separation vortices becomes weaker and the strength of the lower separation vortices becomes stronger. The induced circulation of the lower separation vortices in turn weaken the hull bound circulation caused by the sail tip vortex. As a result, the strength of the normal force acting on the stern section gradually reduced. As the yaw angle increases further, the resulting normal force on stern changes sign and causes the bow to pitch downward

The force and moment results are presented in a coordinate system whose origin is located on the forward perpendicular on the body axis. The x-axis is positive pointing downstream. The y-axis is positive pointing portside and the z-axis is positive pointing downward. This is the coordinate system used in reporting the experimental data. Figure 14 to Figure 19 show the comparisons of the six components of the force and moment coefficients. The comparisons are very good except for the force and moment at the out of plane component at higher yaw angles. This can be caused by the presence of the two struts that are supporting the hull from its side. The struts can generate a circulation on the hull that interacts with the hull bound circulation induced by the sail tip vortex. The interaction may change the normal force on the hull when the yaw angle is sufficiently high.

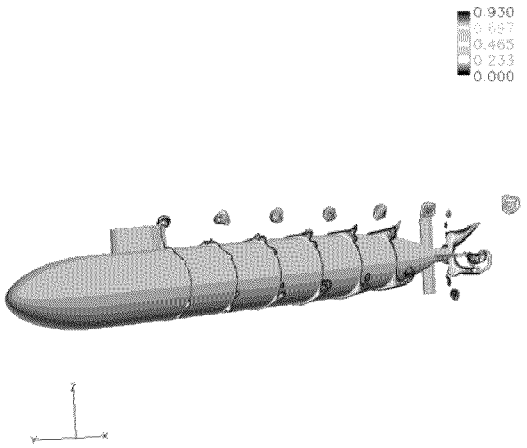

Figure 12: Axial velocity contour along the fully appended hull at 12° yaw.

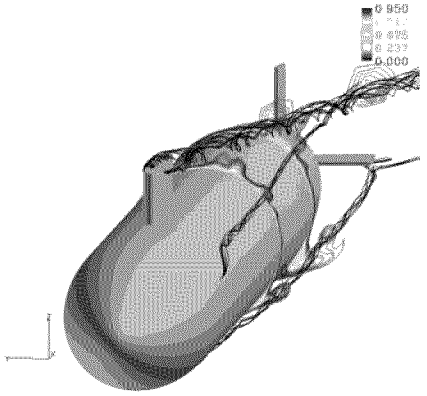

Figure 13: Streamlines emit from the separation lines on sail and hull surface.

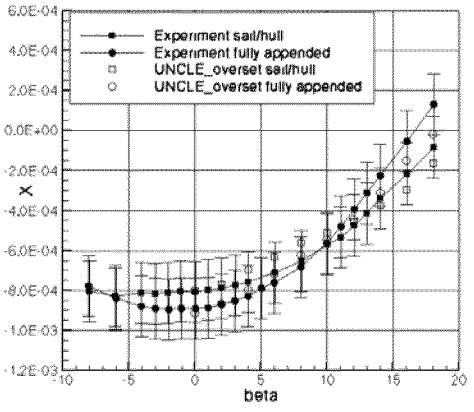

Figure 14: Comparison of longitudinal force coefficient.

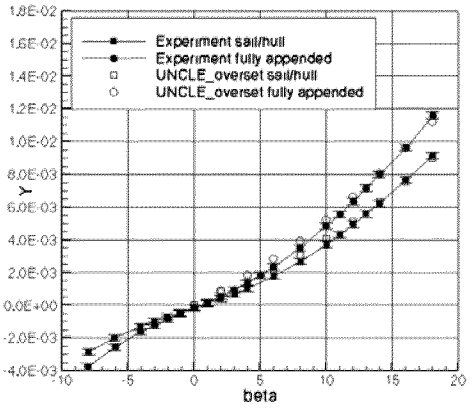

Figure 15: Comparison of lateral force coefficient.

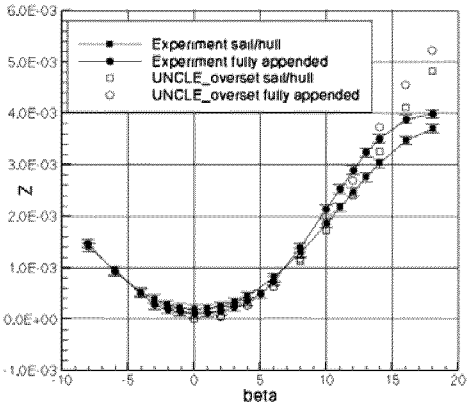

Figure 16: Comparison of normal force coefficient.

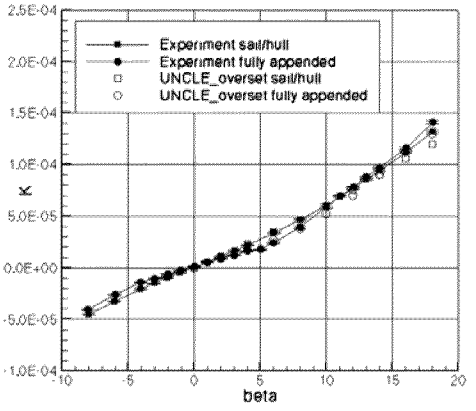

Figure 17: Comparison of roll moment coefficient.

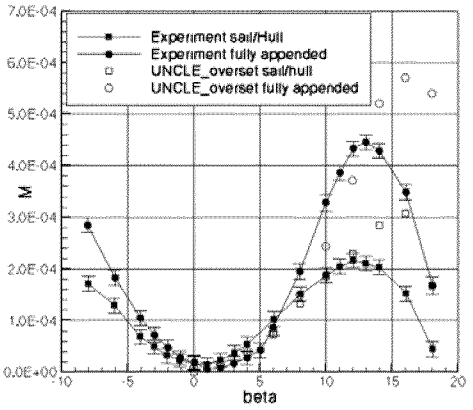

Figure 18: Comparison of Pitch moment coefficient.

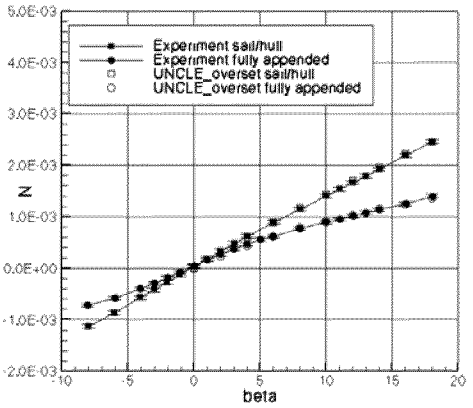

Figure 19: Comparison of yaw moment coefficient.

CONCLUSION

An overset capability was added to the RANS solver UNCLE. The implementation of the capability is greatly simplified by using the DiRTlib and the SUGGAR library routines. The newly acquired capability is validated by simulating the flow over the fully appended ONR-body1.

Some advantages of the overset approach were realized during present flow simulations. It simplifies the grid generation effort considerably for a relatively complicated geometry. The grid systems representing certain physical components can be added and removed from the main body without disturbing the grid systems that represent the remaining components. This allows the study of the hydrodynamic effects and contributions of certain individual components to the overall configuration.

ACKNOWLEDGEMENTS

The U.S. Navy Hydrodynamic/Hydroacoustics Technology Center at NSWCCD provided the high-speed parallel multi-processing computational resources required for the present computations.

REFERENCES

Atsavapranee, P., Forline, T., Frey, D., Hamiliton, J., Percival, S., Sung, C-H, "Experimental Measurements for CFD Validation of the Flow About a Submarine Model (ONR-Body-1)." 25th Symposium on Naval Hydrodynamics. St.John's Newfoundland and Labrador, Canada, 8-13 August, (2004).

Boger, D.A., Dreyer, J.J., "Prediction of Hydrodynamic Force and Moments for Underwater Vehicles Using Overset Grids." 44th AIAA Aerospace Sciences Meeting and Exhibit 9-12January, 2006 Reno, Nevada, AIAA 2006-1148.

Chan, W.M., Chiu, I-T., Buning, P.G., "User's Manual for the HYPGEN Hyperbolic Grid Generator and the HGUI Graphical User Interface." NASA TM-108791, October, (1993).

Chan, W.M., Buning, P.G., "User's Manual for FOMOCO Utilities – Force and Moment Computation Tools for overset Grids." NASA TM-110408 July (1996).

Chan, W.M., "The Overgrid Interfave for Computational Simulations on Overset Grids." AIAA 2002-3188 32nd AIAA Fluid Dynamics Conference. St. Louis, Missouri. 24-26June, (2002).

Chan, W.M., Gomez, R.J. III, Rogers, S.E., Buning, P.G., "Best Practices in Overset Grid Generation." AIAA 2002-3191, 32nd AIAA Fluid Dynamics Conference. St. Louis, Missouri. 24-26 June, (2002).

Chroin,A.J., "A numerical Method for Solving Incompressible Viscous Flow Problems." Journal of Computational Physics, Vol. 2 pp12-26. (1967).

Fu, T.C., Atsavapranee, P., Hess, D.E., " PIV Measurements of the Cross-Flow Wake of a Turning Submarine Model (ONR-Body-1)." 24th Symposium on Naval Hydrodynamics . Fukuoka, Japan, 8-13 July (2002).

Kim, J., "Sub-Visual Cavitation and Acoustic Modeling for Ducted Marine Propulsor." *Ph.D. thesis*, University of Iowa (2002).

van Leer, B., "Towards the Ultimate Conservation difference Scheme II, Momotonicity and Conservation Combined in a Second Order Scheme." Journal of Computational Physics, No.14, pp261-370. (1974)

Noack, R.W., "SUGGAR Users Guide." rnoack@arl.army.mil , January (2005).

Noack R.W., "A Library to Add an Overset Capability to Your Flow Solver." AIAA, June (2005)

Paterson, E.G., Wilson, R.V., Stern, F., " General-Purpose Parallel Unsteady RANS Ship Hydrodynamics Code: CFDSHIP-IOWA." IIHR Report No.432, Iowa Institute of Hydraulic Research, The University of Iowa November (2003).

Rai, M.M.,"Navier-Stokes Simulations of Blade-Vortex Interaction Using High-Order Accurate Upwind Scheme." AIAA Paper 87-0543, (1987)

Rogers, S.E., Kwak, D.,"Upwind Differencing Scheme for Time-Accurate Incompressible Navier-Stokes Equations." *AIAA Journal* Vol.28., No.2, Feb. (1990).

Rogers, S.E., Roth, K., Cao, H.V., Slotnick, J.P., Whitlock, M., Nash, S.M., Baker, M.D., "Computation of Viscous Flow for a Boeing 777 Aircraft in Landing Configuration." AIAA 2000-4221, 18th AIAA Applied Aerodynamics Conference. Denver, Colorado. 14-17 August (2000).
Steger,J.L., Dougherty,F.C., Benek,J.A., "A Chimera Grid Scheme." Advances in Grid Generation. K.N. Ghia, U. Ghia, eds., *ASME FED*. (1983)

Steger,J.L., Benek,J.A., "On the Use of Composite Grid Schemes in Computational Aerodynamics." Computer Methods in Applied Mechanics and Engineering. Vol. 64, pp.301-320. (1987)

Suhs, N.E., Rogers, S.E., Dietz, W.E., "PEGASUS 5: An Automated Pre-Processor for Overset-Grid CFD." AIAA 2002-3186 32nd AIAA Fluid Dynamics Conference. St. Louis, Missouri. 24-26June, (2002).

Taylor, L.K., " Unsteady Three-Dimensional Incompressible Algorithm Based on Artificial Compressibility." Ph.D. thesis, Mississippi State University. (1991).

Wilson, R., Carrica, P., Hyman, M., Stern, F., "A Steady and Unsteady Single-Phase Level Set Method for Large Amplitude Ship Motions and Maneuvering." 25th Symposium on Naval hydrodynamics St. John's, NL, Canada. August 12, (2004)

Yang, C-I, "Numerical Simulation of Flow in Linear Cascade with Tip Clearance." *Hydromechanics Directorate Technical Report* NSWCCD-50-TR-2000/053 (2000)

Yang, C-I, Jiang, M., Chesnakas, C.J., Jessup, S.D., " Numerical Simulation of Tip Vortices of a Ducted Rotor." NSWCCD_50-TR_2004/4. September (2004).